OPEN ACCESS

International
Journal
Of Modern Engineering Research (IJMER)

Processing & Characterization of High Porous Cualni Shape Memory Alloys

Nawal E. Abud Allatif[1], Munther M. Radhy[2], Abass A. Saleh[3]

Abstract:-The necessities for new materials with personalized mechanical and physical properties, has encouraged the study of porous and cellular materials. In our work an open-cell high porous of a CuAlNi SMA is presented.This alloy was produced through a newly suggested process, that involves chiefly in melted metal infiltration of a bed of SiO_2 particles and the following usage of (HF) as dissolvent. The results of Microstructural and compositional analyses displayed that very uniform open-cell high porous alloy could be got, possessing a nearly spherical cell morphology. The energy absorbed by the porous CuAlNi samples was 8.864 MJ/m^3 for 66.26% porosity.

Keyword: SMA, porous CuAlNi, Amorphous Silica gel

I. INTRODUCTION

Today, there is important care from the researcher for a category of materials named stimulus-responsive materials (SRMs), which are capable to respond to a definite motivation, such as, light, heat or chemical. As said by Sun *et al.* , in their paper on SRMs, this sort of materials can be divided into two groups, shape memory materials (SMMs) and shape change material (SCM). Among the types of SMMs is shape memory alloys (SMAs) [1].(SMAs) are metallic alloys that can undergo to alterable martensitic phase transformations as a result of applied thermo-mechanical loads and are capable of recuperating permanent strains as soon as heated beyond an assured transformation temperature. SMAs have actuating and sensing purposes and possess the capability to governor the mechanical properties and replies of their hosts as a consequence of their essential unique characteristics of the shape - memory effect and superelasticty [2].Recently, PSMAs possess attracted considerable attention according to theirbetter mechanical properties with the combined benefits of both porous material and SMAs. Porous shape memory alloys retrieve theapplieddeformationsbecauseeithershape memory effect, during a temperature rise, or pseduelasticty at high temperature. Moreover, the mechanical properties of PSMAs can be regulated by governing the amount of porosity. These properties,alongside interconnected pores ,high damping capacity, high strength, low weight, and low stiffness, make them, encouraging candidates for being applied as bone implants, high weight intelligent systems, and energy absorbers [3].

Diverse methods for manufacturing conventional porous materials and alloys today exist involving casting, powder metallurgy and metallic deposition [4]. Also Cellular metals are fabricated by numerous methods, involving infiltration of molten metal in a leachable solid particle bed as a space holder.

Even today, utmost of porous SMAs were manufactured by powder metallurgy techniques, Several problems arise with these processing methods, comprising the growth of a brittle oxide skin and a difficult governor of (i) the microstructure, (ii) the porous mesostructure [5]Copper based alloys and the Ni-Ti alloys are the solitary two alloy systems that have acquired any grade of commercial investment [6,7]. Properties of the two systems are entirely diverse. Compared to these two sets, the Cu-based SMAs show menial mechanical properties and lower SME is ascribed frequently to the rough grains of Cu-based SMAs. Contrariwise, from the industrial viewpoint, the Cu-based SMAs are considerably further cost-effective than Ni-Ti alloys owing to their inferior manufacturing outlays in addition to their easy fabrication [8].

II. EXPERIMENTAL PROCEDURE

Figure (1) shows the technical flow chart of the experimental work**.**

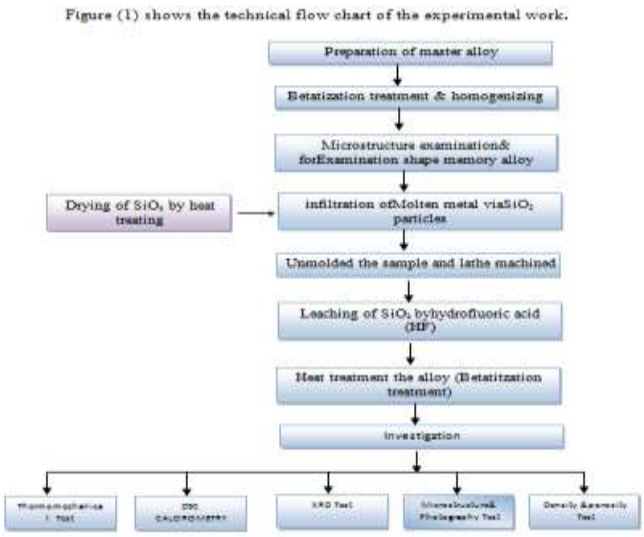

Figure (1): The block diagram illustrated experimental work.

2-1 Materials Used

The starting material (copper, aluminum and nickel) was used to prepare the master alloy Cu-Al-Ni SMAs.

Tables (1), (2) show the chemical composition of copper strips and aluminum rods used, the chemical analysis was done by spark chemical analysis in a Specialized Institute of Engineering and Industries.NickelPowder with purity of (99.8) % was supplied from Seelze-Hannover-Germany

Table (1) Chemical analysis of copper strip

Element	Zn%	Sn%	Fe%	Ni%	Si%	p%	Al%	Cu%
Wt.%	0.043	0.014	0.050	0.86	0.013	0.024	0.062	Balance

Table (2) Chemical analysis of aluminum rod

Element	Zn%	Sn%	Mn%	Fe%	Mg%	Si%	Cu%	Al%
Wt.%	0.017	0.004	0.003	0.217	0.003	0.069	0.037	Balance

Commercial types II 7500 silica-gel beads, [provided from Sigma Ch. Co.] wereutilized as a space holder. The chemical compositionanddensity of the particles are (SiO2>99.7%) and 2.2 g/cm^3 respectively. Melting and boiling point is 1600 and 2230^{o}C respectively.

Silica-gel is ordinarily applied as dried and it is economically obtainable global as an inexpensive material.

Solution ofhydrofluoric acid (25 vol. %) supplied from Solvay Co. by Cardiff University Lab. was applied to dissolve silica gel by wet chemical etching.

Preparation of(CuAlNi) Master Alloy

The Cu-Al-Ni alloy was cast in an electric furnace type Carbolite, under pure Ar flow at room pressure.The alloywas first prepared by melting the copper and aluminum chips with a purity of (> 99%) then added the nickel powder covered with a foil of copper. Flow rate of argon remaining at 0.5 bars / min till the end of melting process. The small amount of sodium fluoride was added to the molten metal during the process and stirring with graphite rod.

Finally, the melt was poured into metallic molds shown in figure (2- b) and left to cool at room temperature.The chemical composition of the product (copper base shape memory alloy (CuAlNi)), that tested by spark chemical analysis in Specialized Institute for Engineering Industries is shown in table (3).

Table (3)the chemical composition of master alloy

Element	Zn%	Pb%	Sn%	p%	Fe%	Ni%
Composition (%)	0.02	0.019	0.019	0.021	0.188	4.1
Element	Si%	S%	Cr%	Al%	C%	Cu%
Composition (%)	0.038	0.013	0.031	13.44	0.073	Bal.

2-3 Preparation of porous SMAs alloy

The melting process has been preceded by using a system designed & fabricated locally by the researcher shown in figure (2); it involves an electric furnace equipped with handle screwed press load, control circuit, thermo couple type k ,protective environment with argon gas and metallic mold.

In order to produce samples with definite porosity and pore sizes, volume fraction of SiO_2 (75) % was considered; for shortness from here it will be called G1.The silica gel sizes were prepared by using a standard sieve with a size range (-2.00+ 2.36) subsequently called F1.

A proper weight of the CuAlNialloy calculated according tothe intended foam volume fraction having almost 25% (G1),was put at the depth of a crucible (100 mm in depth, 35 mm interior diameter), made from graphiteThen amorphous silica oxide spheres were heating prior infiltration in order to get rid of humidity content. The heating achieved by heating at 400 ^{o}C for 30 minutes in the air and then at the 900 ^{o}C for approximately 45 minutes. Then silica gel (space holder) was put on the top of the alloy, as wellinterior the crucible, and lightly shaken for amelioratingpiling.

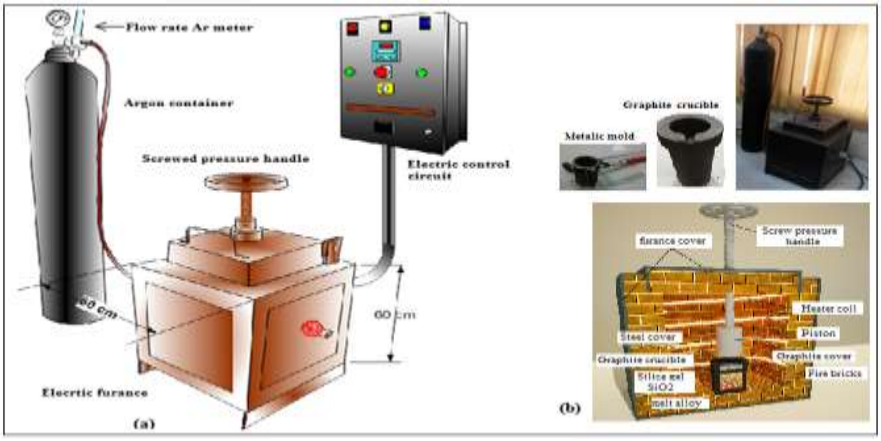

Figure (2) melting system

.

Lastly, graphite disc, stainless steel cylinder and load of 70-90 N were applied on top as a cap, shutting the crucible for superior temperature distribution above the silica beads. Figure (3) illustrates schematically of the preparation steps.

1-The primary formation can be shown on Fig. (3-a). At this point the furnace was turned on and set at 1175 ^{o}C for 150 minutes, the metal was molten. During the period the melting completed after that the major power was switched off and silica-gel bed was compressed down due to the presence of load as shown in figure (3- b).

2- At this stage the infiltrated metal was capable to freeze amongst the silica particles (Figure 3- c). After entire coolingand solidification, the residual solid (silica-gel beads added to infiltrate alloy) was unmolded and machined by lathe to its final format.

3-Leaching of silica gel: Amorphous silica oxide was dissolved by wet chemical etching in aqueous solution of hydrofluoric acid HF (25 vol. %).

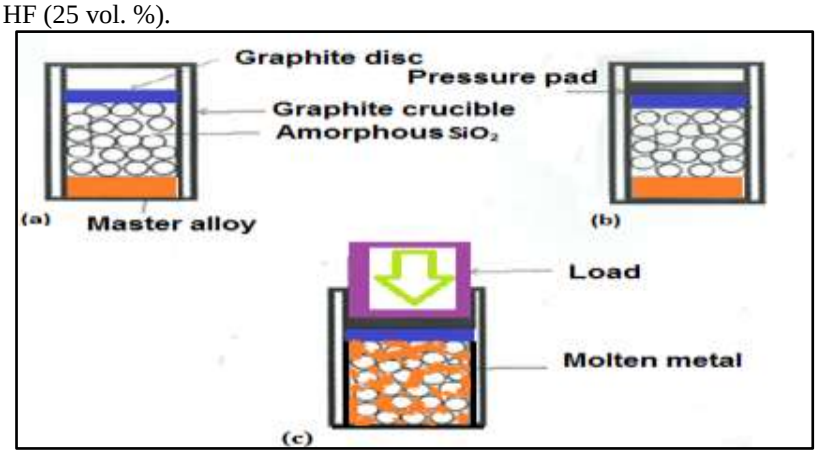

Figure (3) schematic of infiltration process: (a) alloy melting, (b) Pressing of silica gel, (c) infiltration completed

2-4 betatization treatment

The alloy and porous samples were heat treated in a resistance furnace type Carbolite supplied by Cardiff Engineering School (operated at a temperature range of 1000 ^{o}C) .The process accomplished by heating the alloy at the temperature 900 ^{o}C with a heating rate of nearly 30 ^{o}C.Hold for one hour and quenched in water at room temperature.

III. Characterization and Testing

For microstructural observations, the samples was ground by using SiC paper (180, 600,1200 grade paper) with the grinding and polishing Mecapol machine, type 225 U, and polished by using the clothes and Al_2O_3 suspension diamond gel. Later on, the sample is etched for two minutes in a solution composed of 2.5 cm. $FeCl_3$ and 48 ml methanol in 10 ml HCl [9]. The pore size measurements were carried out by the Optical Microscope (OM) type Leica Dmlm.

So as to investigate the microstructure, chemical compositions of prepared samples and take the SEM images.Scanning Electron Microscope equipped with energy dispersive x-ray analysis unit (EDAX) was used. Vickers hardness results were accomplished using a digital hardnessmeasuring device type (Innovatest)).
Compression testing device, type Tinius Olsen, model 602 console, 200k S/L, used with a maximum supporting loads of 1000 KN and a digital display. Compression test involves an axial compression load being applied to a standard specimen of circular cross section (25mm diameter and 33.44 mm high) with a constant head speed at about (2 mm/min) by hydraulic means. The X-Ray diffraction test has been carried out by using Cu-Kα beam with an angle from (20-80)degreewith 45 kV & 40 mA. This investigation has been utilized in order to investigate the phases that might be present by using X-ray powder diffraction (XRD) Inel EQUINOX –Model 3000 some of X-Ray diffraction tests were achieved atLaboratories of the Ministry of Science and Technology and the others in pharmacy School; Cardiff University –Wales-UK

The porosity of the porous shape memory alloy was calculated from the density of the samples. The sample weight was measured by an electrical balance of four digits type (TP - 214), the accuracy of the measurement method is about (0.0001 g).
Archimedes principle was used in measuring the volumes, and the density was calculated for bulk and porous samples.
Relative density of metallic foam (ρ*) can be calculated using the following equation:-

$$\rho^* = \rho_f / \rho_s \text{……..(1)}$$

Where; ρ_f is the density of porous sample (g/cm³), ρ_s represents the solid density (g/cm³)
So the porosity of porous SMAs can be calculated using the following equation [10]:-

$$\text{Porosity (\%)} = 1 - \rho^* \text{…….. (2)}$$

The martensitic transformation cycles andthe starting and finishing transformation temperatures (M_s , M_f , A_s ,A_f) have been determined by differential scanning calorimeter (DSC) device using a DSC 0-600 model PT-1000. (10-25) mg were tested by applying heat and cooling. The first range is heating from (-150 to 250) ^{o}C then returned by cooling with a speed of 10 ^{o}C/min.The martensitic transformation is endothermic during the (martensite β phase) and exothermic during the RT
(β phase $\xrightarrow{}$ Martensite)[11].

IV. Results And Discussion

The microstructure of the as-cast samples was often characterized by the presence of precipitates of the equilibrium phase□. This phase appear as small grains (light gray, mottled) in a matrix of white□ □□ □phase, as shown in figure (4).

After the betatization treatment, the microstructure consists of crystal structure of martenstic phase□ □1($CuAl_3$) orthorhombic appear as needle shape, as shown in figure (5).

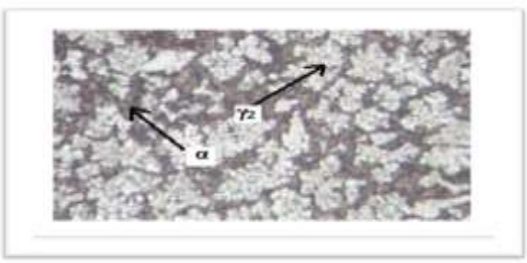

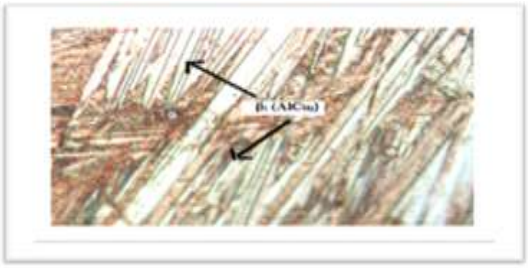

Fig. (4) the optical microstructure **Fig. (5)** the optical of CuAlNi a CuAlNi alloy as castafter heat treatment

Samples were obtained from the experimental work included group with volumetric fraction named G1 (25%) and containing pore size denoted by F1 (-2 +2.36) mm.A cylindrical parcel outcome of metal and amorphous silica-gel beads after solidification and is shown in Figures (6).

Typical sections of the prepared porous sample and the final product are shown in figures (7).


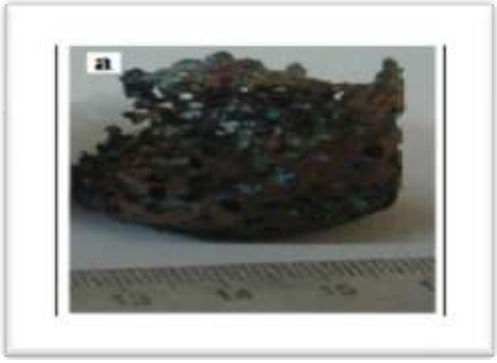

Fig. (6) Infiltrated silica gel bed afterFig. (7) typical sections of cooling sample G1with pore size F1porous CuAlNi alloy with F1 Pore size

Figure (8) illustrate a SEM image of a heat treated specimen. The infiltrated space holder spheres can beobviously seen.
Figure (9) shows a SEM image of the polished specimen surface. It is possible to see the uniform pore distribution of nearly spherical cells, in addition to many interconnecting windows.

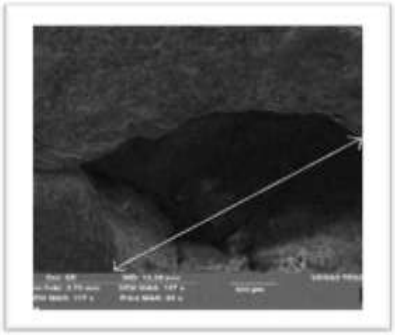
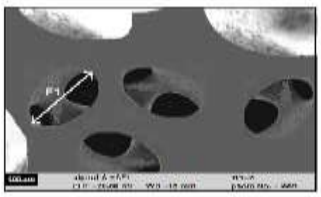

Fig. (8) SEM image of heat treated Figure (9) SEM polished photographporous CuAlNi alloy CuAlNi alloy surface

Also, it can be realized from the figures that silica gel were thoroughly leached by fluoric acid, without visual signal of any considerablealloy corrosionand no vestige of Silicon and oxygen on metal ligaments after leaching silica gel.This demeanor was in prospect and it is in conformity to the chemical and mechanical stability of silica gel beads at the selected processing temperature (maximumprocessing temperature 1175 ^{o}C). It is clear from the images that silica gel beads almost stayed in its original shape and size during infiltration.
EDS analyses present no inter-diffusive phase or reaction products between alloy and silica gel spheres and also show an outstanding uniformity of the chemical composition both in porous and bulk samples as shown in figures (10) & (11).


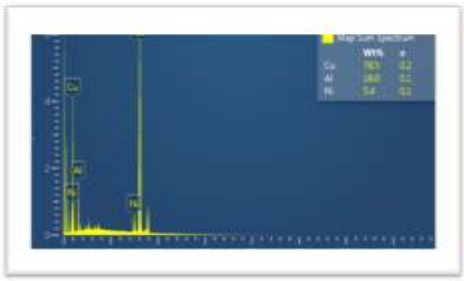

Fig.(10) SEM image of the metallicFig.(11) EDS spectrum image of the ligament after leaching of SiO_2metallic ligament afterleaching

Of SiO_2

Figures (12) & figure (13) clarify respectively the X-ray diffraction (XRD) patterns of the as-cast CuAlNi sample structure, solution heat treated sample (soaking at 900 °C for one hour followed by quenching in water).

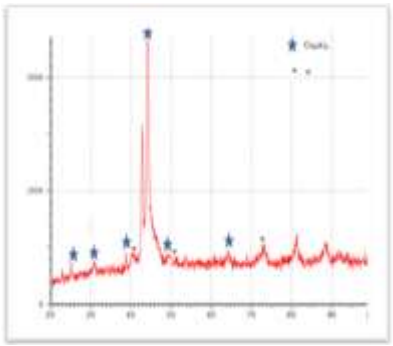

Fig. (12) XRD profile of as cast CuAlNi alloy

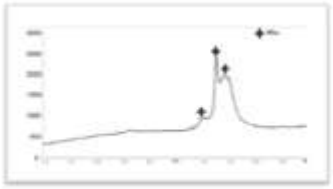

Fig. (13) XRD profile of the CuAlNi alloy afterbetatization

Considering Figure(12),theX-ray diffraction result corroborates the existence of γ_2 (Cu_9Al_4) compound in addition to α (Cu-Al-Ni) solid solution. This denotes that β phase endures the eutectoid decomposition of β→α+γ2 due to slow cooling rate. This behavior coincides with phase diagram of CuAlNi and researcher work [12]. Figure (13) displays the X-ray diffraction pattern of the CuAlNi alloy Solution heat treated at 900 °C for one hour followed by quenching in water.Clearly, the matrix comprises of β_1 martensite phase that has a crystal structure orthorhombic. It appears as a result of quenching rapidly from high temperature. The *β*1low intensity peaks show that there is a certain unchanged austenite phase. This has been observed by several researchers [13, 14].

Porous CuAlNi specimens, with definite pore cell size and volume fraction, were processed and characterized. Figure (14), displayed small interconnection windows between neighboring pores. That means, for the duration of the infiltration method, the amorphous SiO_2 beads utilized as space holders be there not entirely damp by molten alloy, that left some unfilled interstitial space. This situation makes open-cell structure in the porous status, needful to gain comprehensivespace holders dissolution.

Furthermore, since the interior surface of the cells is a ‘‘negative photograph’’ of the superficies morphology of the SiO_2 spheres, it is conceivable the size allocation of cells and space holders, can be regarded to be officially similar.

As can be shown from figure (14), amorphous SiO_2 beads were thoroughly disintegrated by hydrofluoric acid, without visual substantiation of any considerable alloy corrosion. From these photographs, it is potential to estimate that the SiO_2 beads did not exposed any alteration in their primary size/shape through either metal solidificationor infiltration .

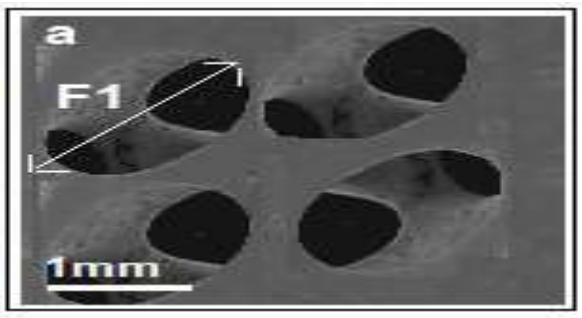

Fig. (14) SEM image of CuAlNi polished G1 specimen surface with F1 pore sizes

The weighing and measuring method used for evaluating the material porosity granted reproducible outcomes: rate values are summarized in Table (4). The porous samplepresenteda vacant space proportion a bit higher than the theoretical, which consort to arbitrary packing of vibrating hardspheres of the same size. This consequence can be partly demonstrated as an outcome of the non-entire damp ability of amorphous SiO_2 beads by molten alloy that leaves amount of the unfilledinterstitial space, equating certain piling faults.

Table (4) Porosity and relative density of processed specimen

Pore size range, mm	Average porosity, %	Relative density
2-2.36	71.3	0.28

Calorimetric tests were achieved on samples of around 25 mg. The outcomes display the transformationtemperatures. The values tabulated in Table (5) present transformation temperaturesof the as-cast state and after the heat treatment. In the bulk heat treated condition, the inspected alloy has anacute transformation peak,such as visualized in Figures (15). DSC scans of the porous G1F1 sample after heat treatment ameliorates the transformation conduct and shifts DSC peaks to higher temperatures as shown in figure (16). After the molten metal infiltration process, widertransformation peaks are noticed in the temperature range recorded in Table (5).

Table (5) DSC results for a bulk and porous specimens (heat treated)

Sample	M_s (^{0}C)	M_f(^{0}C)	A_s(^{0}C)	A_f(^{0}C)	M_s- M_f (^{0}C)	A_f - A_s (^{0}C)
BM	**24**	**5**	**10**	**33**	**19**	**23**
G1F1	**30**	**6**	**12**	**34**	**24**	**22**

Sample	M_s (^{0}C)	M_f(^{0}C)	A_s(^{0}C)	A_f(^{0}C)
BM	**24**	**5**	**10**	**33**

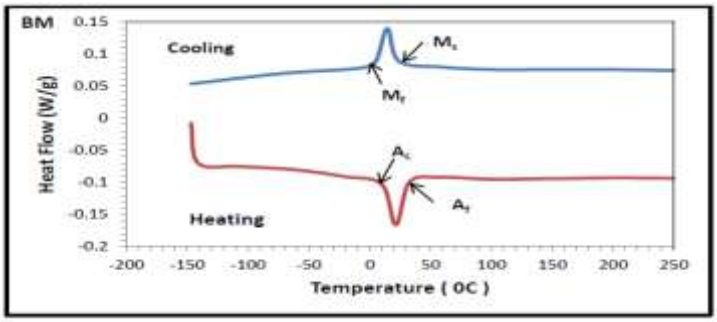

Figure (15) DSC profiles of BM specimens

This appearance is probably related with substantial heterogeneity of the DSC samples because those were selected from diverse sites in the porous SMA.
Probably, possible dissimilarity in the morphologyor microstructure of the examined DSC specimens may influence theshapeand intensity of the peaks instead of the transformation start and end temperatures.

In addition, remaining interior stresses, which could engender in the porous shape memory alloy sample during quenching in water and would vary relying on space holder's sizes, may change the peak intensities this result is confirmed by the references [15].

Sample	M_s (^{0}C)	M_f(^{0}C)	A_s(^{0}C)	A_f(^{0}C)
G1F1	**30**	**6**	**12**	**34**

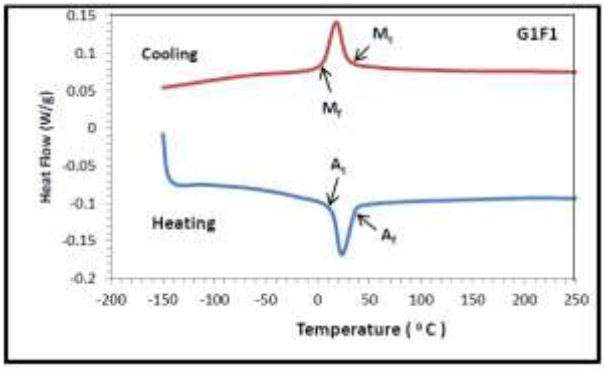

Figure (16) DSC profiles of porous G1F1 specimens

4-1 Thermo-Mechanical Compression Test

Pseudoelasticty tests were achieved on both of bulk CuAlNi alloy and porous samples on testing machine Tinius Oisen type (H100KU).Pseudoelasticty tests were carried out at a steady temperature of 60 ^{o}C, in order to retain the sample in the austenitic condition, and increasing magnitudes of strain, at a deformation speed of 0.2 mm/min.Bulk samples, deemed as the reference substance, presented an entire retrieval of strains until

2.5% figure (17) and figures in appendix B, but for increasing deformation amounts, the remaining strain became pertinent as shown in figure (18).Figure (19) illustrate the compression test of the bulk sample and it is clear that the maximum load is 314KN, by using the definition ofCompression stress equal to force over the area (cross sectional area)also strain (ε) equal to change in heigh over the high of the specimen,it obviously indicates that compression stress and yield stress is 640MPa and 440MPa) respectively this confirm with the reference [16].From figures (17),figures (18) &figures (19) the values of stress and strain are determinedand the same thing for others are doing and tabulated inin table (6).

Table (6) the values of compression stress and strain of bulk alloy

Sample	BM							
Max. Load (KN)		13.159	30.5	51.2	78.5	133.5	175	220
Stress (Mpa)		26.855	62.244	104.489	160.204	272.449	357.14	448.979
Δℓ(loading)	0.334	0.501	0.668	0.836	1.003	1.3376	1.672	2.006
Strain (ε)%	1	1.5	2	2.5	3	4	5	6
Residual strain (Δεr)	0	0	0	0	0.617	1.15	1.68	1.78
Δεmax.	1	1.5	2	2.5	3	3.38	3.23	2.55
Δεr/Δεmax.	0	0	0	0	0.16	0.34	0.52	0.7
Index for recovery	1	1	1	1	0.84	0.66	0.48	0.3

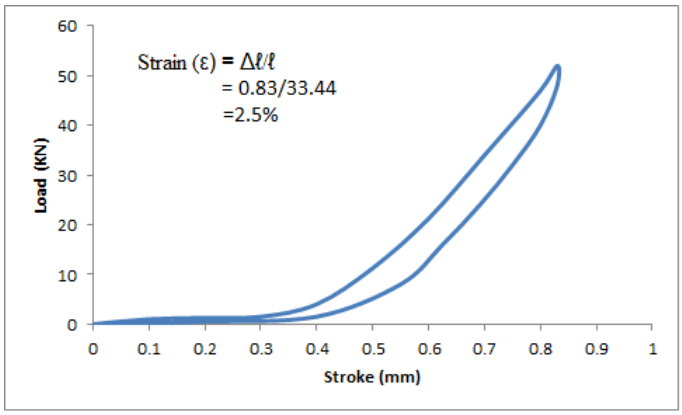

Figure (17) pseudoelastisity compression test profile; for as cast CuAlNi (bulk) alloy ε=2.5%

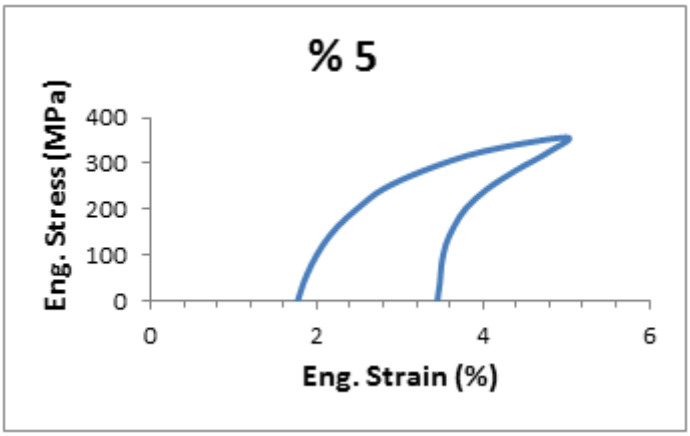

Figure (18) pseudoelastisity compression test profile; for as cast CuAlNi (bulk) alloy ε=5%

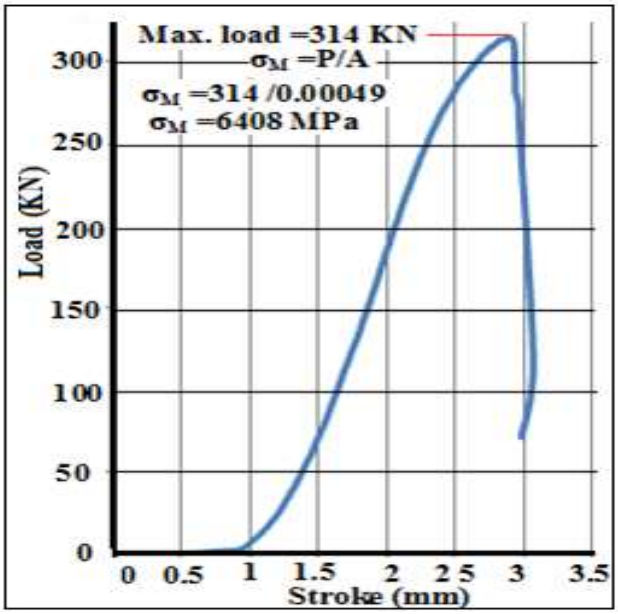

Figure (19) compression test profile; for as cast CuAlNi (bulk) alloy (maximum load)

Thermomechanical test of porous specimen show that Porous alloy were not capable to completely retrieve the used strains even at low deformation magnitudes, This is can be attributed to localized plasticity which can take place much less the comprehensive compressive strength of the porous specimens[17].

In spite of this truth, the capability to retrieve greater strains (over 4%) of porous with smaller sizes of pores (F1) was superior while compared to that of the bulk, possibly owing to irreversible slipping of grain surfaces, taking place in the bulk specimens (Figures, (20), (21), (22), (23), and (24).

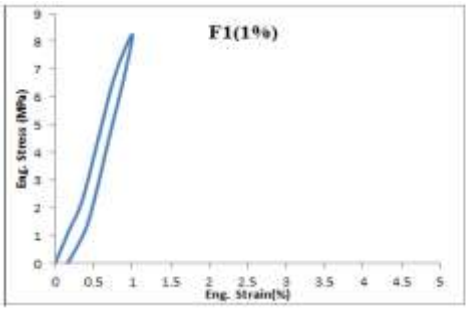

Figure (20) PE compression test profile F1 porous specimen (1%) F1 (pore size range 2-2.36 mm)

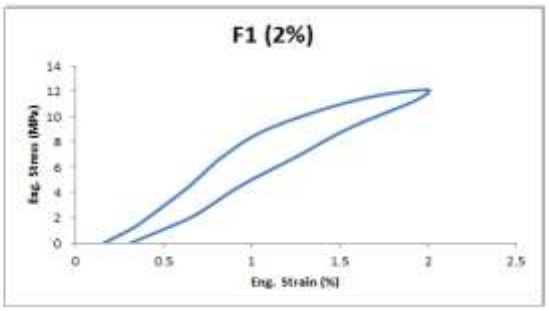

Figure (21) PE compression test profile F1 porous specimen (2%) F1 (pore size range 2-2.36 mm)

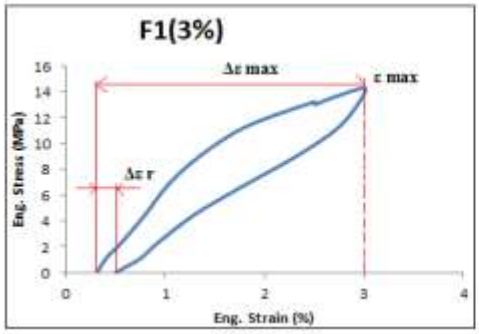

Figure (22) PE compression test profile F1 porous specimen (3%) F1 (pore size range 2-2.36 mm)

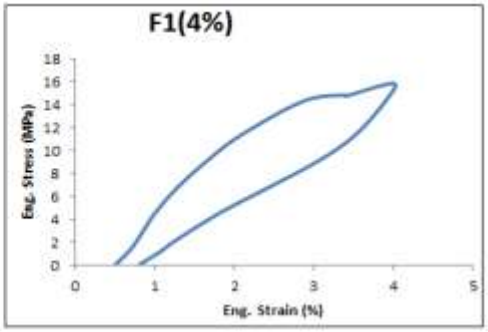

Figure (23) PE compression test profile F1 porous specimen (4%) F1 (pore size range 2-2.36 mm)

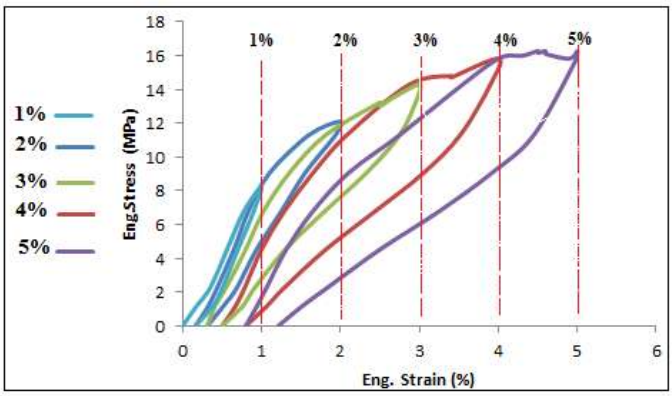

Figure (24) PE compression test profile of porous CuAlNi SMA with pores size F1 (pore size range 2-2.36 mm)

As noticed in the pseudo elasticity tests, porous samples displayed worse performance at small strains (3%), but the porous offered better index results of recovery at upper strain magnitudes when it compared with a bulk specimen; summary results of pseudoelasticty compression tests are shownin table (7)and in figure (25).

Table (7) pseudoelasticty compression tests summary results

Samples	Porousalloys(withpore size F1)						
εmax (%)	1	2	3	4	5	6	7
Max stresses (Mpa)	8.249	12.091	14.2945	15.82	16.272	16.662	16,872
Δεmax (%)	1	1.93	2.6212	3.018324		6	3.58
Δεr (%)	0.07	0.3088	0.602876	0.905497		3.42	2.7566
Δεr/Δεmax.	0.07	0.16	0.23	0.3		0.57	0.77
1-Δεr/Δεmax.	0.93	0.84	0.77	0.7	0.56	0.43	0.23

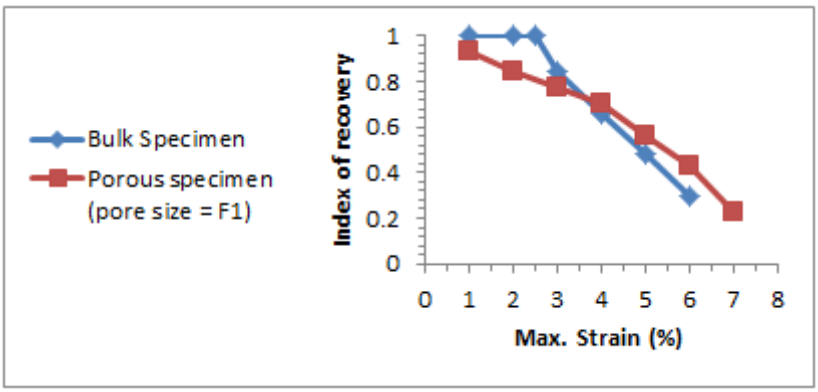

Fig. (25) Pseudoelasticity tests summary results

4-2 Energy Absorbing:

Up to now, cellular metals are principally used in energy absorption arenas. Energy absorption capacity is one of the significant aspects to estimate the characteristic of porous copper-aluminum-nickel SMA. In this contribution they were calculated according to Eq. (1) [17].

$W = \int_0^{\varepsilon} \sigma d\varepsilon$ …….. (1)

Where W is the energy absorption capacity, σ is the stress where the stain is ε. The total energy absorption capacity (defined as the energy absorbed when strain reaches the densification strain.

Porous CuAlNi specimens submit plastic deformation with typical yielding when it is exposed to an external compression load.

Figure (26) shows a schematic stress–strain curve for compressionporous SMA specimen. Obviously there was a wiggle of the plateau stress during plastic deformation regions. This could be owing to the non-homogeneity of high porosity samples and / or weakness of the cell wall**.**

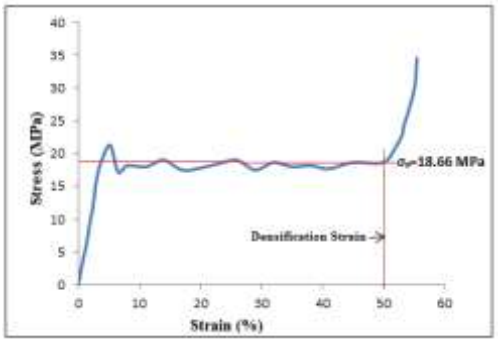

Figure(26)Stress strain curve for porous CuAlNi samples .

It is clear that stress increases linearly to a value of 18.66 MPa in the range of strain from (0 – 5%), an upper yielding point (A) and a lower yielding point, which are typically characteristic of porous metals.Yet stress remains constant, while the strain has largely increased till 50% strain. After this point the stress proportionally increases by a small amount of strain change.The illustration this demeanor of curve denotes that porous sample had been deformed elastically, the stress rises up to local peak stress, in the first region (0-5%) strain and then plastic deformation started at 18.66 MPa and continued with stress constancy. This type of deformation continued throughout the region two (5%-50%) strains. Eventually, the proportional increase of stress with a few percent of strain change (region three) was owing to the fact that the porous samples behave as a solid matter because the porous cells were entirely destroyed and densification had taken place (18).
The energy absorbed by the porous CuAlNi samples which had been calculated from the area under the stress – strain curves was 8.864 MJ/m^3.

V. Conclusion

From the present work, the main Conclusions which can be drawn are:-

1-The microstructure of as cast (Cu13.44% wt. Al 4.1%wt. Ni) bulk and porous samples are □□(Cu $_9Al_4$)compound and α (Cu-Al-Ni) solid solution. And single martensite phase($AlCu_3$)appear after betatization treatment.

2- The results showed given porous CuAlNi shape memory alloy can be dependably and advantageously produced with definedpore size (-2.0 + 2.3) mm.

3- The empirical work appeared amorphous silica gel stay stable in shape and size during liquid infiltration (processing temperature 1100 ^{o} C). Owing to the high chemical stability of SiO_2 particles & no interaction has been found with the system during liquid infiltration. Also amorphous SiO_2 grains were entirely dissolved by an aqueous solution (25%) hydrofluoric acid, without visual evidence of a chemical attack of the metal.

5- The resulting porosity of porous CuAlNi shape memory features is found to be homogeneous with space-holders (-2.0 + 2.3) mm are used and most of the observed cells are open and interconnected.

6- Calorimetric analysis showed the transformation temperatures for the bulk material are (M_s =24 ^{o} C), (M_f =5 ^{o} C), (A_s =10 ^{o} C), (A_f =33 ^{o} C). And for the samples G1F1 (M_s =30 ^{o} C), (M_f =6 ^{o} C), (A_s =12 ^{o} C) , (A_f =34 ^{o} C). That is indicated, no important differences between bulk and porous samples; the main effects of the betatization treatment were found to be a shift in transformation temperatures to higher values.

7. Compression testing revealed that the porous structure has affected by the morphology of the voids and failure take place above a critical value of σ_{pl} (18.66 MPa, which is found lower than expected value according to well-known relationships among bulk properties and foam properties. At low deformation levels (2.5 %) pseudoelastic recovery of deformation is superior for bulk samples (100 %) than for the porous, at higher strains (5% and 6%) the performance of pores (-2.0 + 2.3) mm foam is better (56% and 43%), compared to the bulk which are 48% and 30% respectively.

9-It can be shown from the results that the energy absorbed by the porous CuAlNi samples was 8.864 MPa for 0.33 relative density

References

[1]. Mohammad Amri Zainal, Shafishuhaza Sahlan and Mohamed Sultan Mohamed Ali "Micromachined Shape-Memory-Alloy Microactuators and Their Application in Biomedical Devices"Micromachines 2015, 6, 879-901

[2]. Article, R. (2014). "A concise review of the applications of NiTi shape-memory alloys in composite materials", 110(7), 5–9

[3]. M. R. Karamooz Ravari, M. Kadkhodaei, and A. Ghael "Aunit cell model for simulating the stress-strain response of porous shape memory alloys" Journal of materials engineering and performance ,2015

[4]. Alaa Abdulhasan Atiyah, Abdul-Raheem Kadhum Abid Ali, Nawal Mohammed Dawood "Characterization of NiTi and NiTiCu Porous Shape Memory Alloys Prepared by Powder Metallurgy (Part I)" Arabian Journal for Science and Engineering March 2015, Volume 40,Issue 3, pp. 901-913.
[5]. B. Gadot, O. Riu Martinez, S. Rolland du Roscoat, D. Bouvard, D. Rodney, L. Orgeas " Entangled Single-Wire NiTi Material: a Porous Metal with Tunable Superelastic and Shape Memory Properties" Acta Materialia May 12, 2015
[6]. W. M. Huang, Z. Ding, C. C. Wang, J. Wei, Y. Zhao, H. Purnawali "Shape memory materials" Materials today July-august 2010 Vol. 13 No. 7-8 pp.54-61
[7]. Dr. Abdul Raheem. K. Abid Ali & Zuheir T. Khulief.Al-Tai "The Effect of Iron Addition on the Dry Sliding Wear and Corrosion Behavior of Cu Al Ni Shape Memory Alloy"Eng.& Tech. Journal, Vol.28,No.24,2010
[8]. Izadinia, M., & Dehghani, K. "Structure and properties of nanostructured Cu-13.2Al-5.1Ni shape memory alloy produced by melt spinning". Transactions of Nonferrous Metals Society of China, (2011),Vol.21(9), pp. 2037–2043
[9]. In, M., Analiza, F., Zlitine, S., Goji, M., Ko, S., An, I., … Kosec, B. (2013). "Microstructural and Phase Analysis of CuAlNi Shape-Memory Alloy After Continuous Casting",Vol. 47(2), 149–152.
[10]. N. G. Wadley, "Cellular Metals Manufacturing", Advanced Engineering Materials, vol. 2, No.10, 2002, pp.726-733
[11]. Ortin J, Planes A. "Acta Metall "1988; Vol.36: PP.2417
[12]. Hamouda, K., Chentouf, S. M., Bouabdallah, M., Cheniti, H., & Amimer, N. (2013). "Nanometric AlNi Precipitation in a 84.68 wt.% Cu-11.25 wt.%Al-4.07 Wt%Ni Shape Memory Alloy. Defect and Diffusion Forum", 334-335, 1–6.
[13]. Alloys, T. C. S., & Juan, J. S. A. N. (2002). "Influence of Al and Ni Concentration on the Martensitic",Vol. 33(August).
[14]. Ali M. Mustafa "Studying Shape Memory Effects of Cu-Al-Ni Alloys"PhD Dissertation /Univeristy of technology/Departement of Metallurgical Engineering,2014
[15]. M. Stipcich, R. Romero, "The effect of Ti-B on stabilization of Cu-Zn-Al martensite", Mat. Sci.Eng. A273-275 (1999) 581-585
[16]. Engineering, E. (n.d.). Shape-Memory Alloy Devices in Earthquake Engineering : Mechanical Properties , Constitutive Modelling, (September 2003).
[17]. M.F. Ashby, A. Evans, N.A. Fleck, L. Gibson, J.W. Hutchinson, and H. Wadley," Metal Foams: A Design Guide", Butterworth-Heinemann, Boston, 2000
[18]. Hall, I. ., Guden, M., & Yu, C.-J. (2000). "Crushing of aluminum closed cell foams: density and strain rate effects". Scripta Materialia, 43(6), 515–521.